VI International Conference on Computational Methods in Marine Engineering
MARINE 2015
F. Salvatore, R. Broglia and R. Muscari (Eds)

PERFORMANCES ANALYSIS OF A SEMI-DISPLACEMENT HULL BY NUMERICAL SIMULATIONS

D. DURANTE*, R. BROGLIA* AND G. BIZZARRI†

* Maritime Technology Research Institute (CNR-INSEAN)
National Research Council
Via di Vallerano 139, 00128 Rome, Italy
e-mail: danilo.durante@cnr.it/

† Azimut-Benetti S.p.A.
Via Michele Coppino, 104 55049 Viareggio - Italy
e-mail: giovanni.bizzarri@azimutbenettigroup.com/

Key words: Computational Methods, Marine Engineering, Planing Hull

Abstract. The flow field generated by the towing of a semi-displacement hull, free to heave and pitch, is numerically investigated in the velocity range $18 - 34$ Kn. The numerical code adopted is the in-house developed Xnavis, which is a general purpose unsteady RANS based solver; the solver is based on a Finite Volume approach together with a Chimera technique for overlapping grids and a Level Set approach to handle the air/water interface. The generated wave pattern shows many interesting features with an evident wave plunging near the hull bow, while the stern remains completely dry for velocities over 30 Kn. The numerical outcomes are discussed in terms of total resistance, sinkage and trim.

1 INTRODUCTION

The study of semi-displacement and planing vessels is an actual topic since the wide applications range, spanning from sport competitions to patrol boats. From a physical point of view, the high speed reached by these vessels implies a complex interaction between the structure and the free surface of the fluid with a complicate wave pattern developed downstream. The impact of the vessel on the water surface during its motion gives rise to a jet formation with a significant air entrapment and bubbles production. Actually the side jet is substantially definable in terms of a spray sheet, the dynamics of which is highly difficult to study both in experimental and numerical approaches. A lateral chine is intended to throw spray to the sides of the hull, to prevent water from rising up the hull sides and to create a smooth ride in seaway; moreover chines with a wide flat area (called chine flats) contribute significantly to create lift in the moving boat.

In the framework of a numerical approach, an important contribution has been recently addressed by Akkerman *et. al.* (2012) where an investigation at different Froude numbers was carried out on a Fridsma planing hull through a ALE-VMS approach. A comparison with the experimental data showed a good agreement for low Froude numbers, while discrepancies of $10 - 12\%$ are found on high speed cases.

The free surface bow flow around a fast and fine ship in calm water was studied in Landrini *et. al.* (2012) with an emphasis on generation and evolution of the breaking and splashing bow wave using the $2D + t$ theory. A validation was performed through comparison with experimental data and other numerical solutions available in the literature. The DDG51 vessel was used to carry on a parameter investigation in terms of the ship speed (Froude number) and surface tension. The influence of the Froude number on the patterned morphology and the importance of surface tension for small-scale ships in inhibiting the jet formation and evolution were verified.

The impact on the free surface during the hull motion (especially in waves) inspired a long number of works: from a numerical point of view Iafrati & Broglia (2008) and Broglia & Iafrati (2010) studied the effect of the impact of a symmetric and an asymmetric wedge on the free surface through a Finite Volume approach evaluating the wave pattern generated and the jet dynamics; Fu *et. al.* (2012) exploited an immersed boundary approach together with a VOF method (the Numerical Flow Analysis (NFA) code) for the study of the forces and moments on a deep-V planing craft. The impact of a wedge on the free surface was numerically simulated and experimentally validated as test case. In Fu *et. al.* (2014) results from a collaborative research effort involving the Computational Fluid Dynamics (CFD) codes CFDShip-Iowa and NFA were presented and discussed to examine the hydrodynamic forces, moments, hull pressures, accelerations, motions, and the multiphase free surface flow field generated by a planing craft at high-speed (Froude number $Fr = 1.8 - 2.1$) in calm water and waves. The steady forward speed test were performed for two kind of hulls: a prismatic and a double-stepped planing hulls. The sinkage and resistance were in good agreement for the two codes for the last configuration. The irregular wave simulations were carried out with CFDShip-Iowa and compared with experiments, showing a well modelled overall behaviour. Moreover, in Brizzolara & Serra (2007) an extensive study using an up to date RANSE VOF solver with free surface tracking capability was performed, testing the method on a wedge shaped prismatic planing hull, having a constant deadrise angle of 20 degrees, systematically varying the running trim angle and wetted length. Results obtained, in terms of drag lift forces and longitudinal trimming moment, were compared with available experimental and semi-empirical theories.

From an experimental point of view Begovic *et. al.* (2014) appraised the effect of deadrise angle variation along the hull length on seakeeping characteristics in regular waves for one monohedral and three warped models with deadrise angle linearly varying along the hull length with the aim to get an insight on motion and acceleration properties connected with warped hull forms and to provide a benchmark for CFD of planing hulls.

In Judge & Ikeda (2014) a four foot berglass planing hull model was tested in calm water, regular and irregular waves. For each test run, the model motion and the water spray were recorded using high-speed video, the impact pressures were recorded using pressure sensors arrayed on the model bottom, the model accelerations were recorded at the bow. The examination of the wave impacts of the model was carried out as a sequence of individual impact events.

In the present paper, the towing simulations of a semi-displacement vessel are carried out for Fr spanning from 0.6 to 1.2; sinkage and trim, and resistance curves are evaluated.The numerical computations have been pursued by using the unsteady RANS solver χnavis, which is a general purpose simulation code developed at CNR-INSEAN. The code yields the numerical solution of the unsteady Reynolds averaged Navier Stokes equations for unsteady high Reynolds number (turbulent) free surface flows around complex geometries. The solver is based on a finite volume formulation with conservative variables co-located at cell center. The spatial discretization of the convective terms is done with a third order upwind based scheme, whereas the diffusive terms are discretized with second order centered scheme and the time integration is done by second order implicit scheme (three points backward). The solution at each time step is computed iteratively by a pseudo-time integration that exploits an Euler implicit scheme with approximate factorization, local pseudo time step and multi-grid acceleration. Several turbulence models have been implemented in the code, ranging from the one equation Spalart and Allmaras model, to the two equation $k-\varepsilon$ model as well as DES and DDES hybrid models. Free surface effects are taken into account by a single phase level-set algorithm. Complex geometries and multiple bodies in relative motion are handled by a dynamical overlapping grid approach. High performance computing is achieved by an efficient shared and distributed memory parallelization.

Figure 1: Azimut Grande 95RPH

2 PROBLEM ASSESSMENT

In the present paper, the towing of the semi-displacement sailing yacht *Azimut Grande 95RPH* (figure (1)) is simulated. The geometric characteristics as well as the displacement of the vessel are outlined in table (1). The global towing force is reduced to the center of gravity, the vertical and horizontal components of which are $-D\tan(\varepsilon+\varphi)$ and $-D$ respectively where D is the drag force and φ is the trim angle. Moreover, the vessel is towed along the propellers axis line, being f the distance respect to the center of gravity G, so a torque $-fD/\cos(\varepsilon+\varphi)$ is applied also. The sketch of the towing setup is reported in figure (2). The sinkage and trim are assumed free and nine simulations spanning

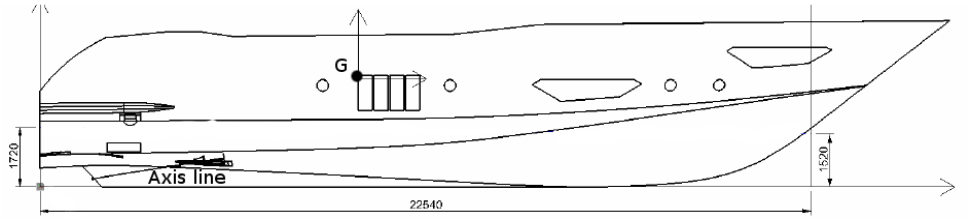

Figure 2: Hull longitudinal profile

Length between perpendiculars	L_{pp}	22.54 m
Displacement	Δ	104 t
Longitudinal position of G	LCG	9.3 m
Vertical position of G	VCG	3.12 m
Propeller axis inclination	ε	9.08°
Distance between G and propeller axis	f	1.634 m

Table 1: Hull characteristics.

from 18 to 34 knots are carried out, the corresponding Froude and Reynolds numbers varying in the range $[0.623; 1.176]$ and $[2.09\,10^8; 3.94\,10^8]$, respectively. An overview of the computational mesh is shown in figure (3); in the figure chimera cells have been hidden for the sake of clearness. In order to obtain a high and accurate refinements close to the hull and skeg, the domain has been discretized by 86 body–fitted patched and overlapped blocks, for a total of 4,670,464 cells. A multigrid technique is exploited in order to achieve a faster convergence to the solution in the pseudo-time; four levels of computational mesh are used. Every level is obtained from the finer one, by removing every other point along each spatial direction. Grid distribution is such that the thickness of the first cell on the wall is always below 1 in terms of wall units, and at least 20 cells are within the boundary layer thickness ($y^+ = O(1)$, i.e. and $\Delta/L_{pp} = O(20/Re)$, Δ being

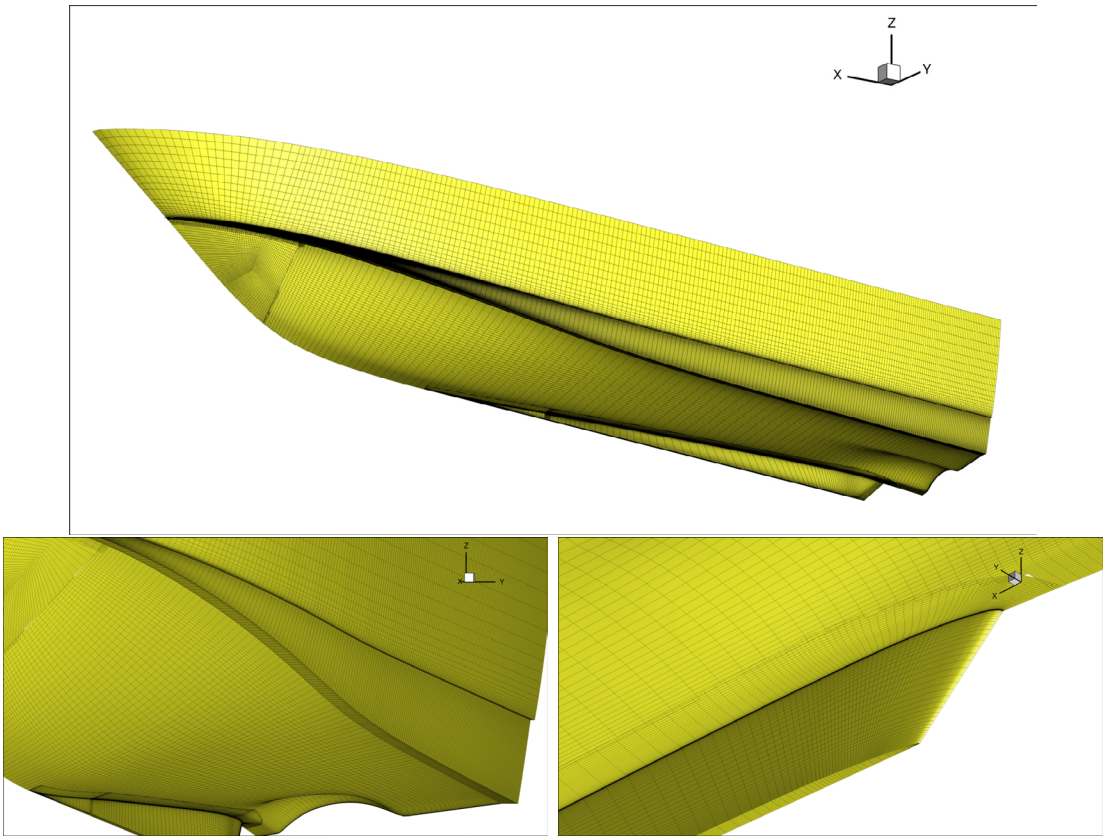

Figure 3: Computational mesh around the hull: the skeg and the chine are magnified.

Zone	N. of Cells
Background near	518,656
Background far	141,312
Hull	844,800
Bow	262,144
Center	1,075,200
Stern	192,000
Transom	1,148,928
Skeg	487,424
TOTAL	4,670,464

Table 2: Mesh cells distribution

the thickness of the cell). Size and position of the 86 structured blocks in the domain are listed in table (2). As visible in the top plot of fig. (3), the hull is characterized by an hard chine along the vessel (useful for deflecting the sprays, as outlined in the Introduction)

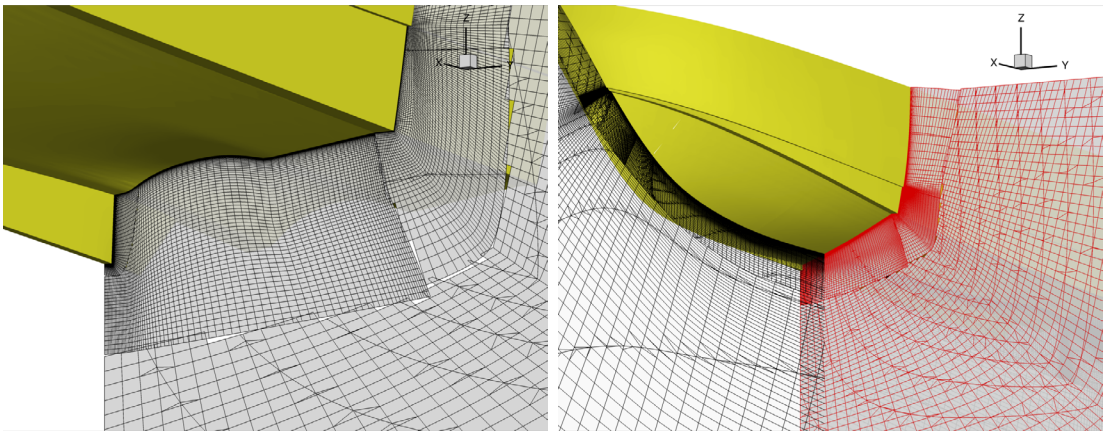

Figure 4: Slices of the computational mesh around the hull: the skeg and the chine are magnified.

and an aesthetic chine over it.

An important effort was spent for the modelling of the chines and of the skeg that looks very thin and narrow. In fig. (4) some slices of the numerical domain highlight the important stretch of the grid volumes near the walls and the overlapping of sets with different topologies: the chimera cells have been hidden for the sake of clearness.

The numerical solutions were computed by means of a Full Multi Grid-Full Approximation Scheme (FMG-FAS) (see Favini *et. al.* (1996)), with four grid levels, each obtained from the next finer by removing every other grid points; the three finest grids (for which the refinement ratio is 2) have been used for Verification and Validation purposes. In the FMG-FAS approximation procedure, the solution is computed on the coarsest grid level first; then it is approximated on the next finer grid and the solution is iterated by exploiting all the coarser grid levels available with a V-Cycle. The process is repeated up to the finest grid level. On each level, the iterative solution is carried on until the L_2-norm of the residuals drops of four orders of magnitude and the variation on the forces and moment is at most on the fourth digit.

3 NUMERICAL APPROACH

The governing equations for the unsteady motion of an incompressible viscous fluid can be written in integral form as:

$$\begin{aligned} &\oint_{S(V)} \boldsymbol{U} \cdot \boldsymbol{n}\, dS = 0 \\ &\frac{\partial}{\partial t}\int_V \boldsymbol{U} dV + \oint_{S(V)} (\boldsymbol{F}_C - \boldsymbol{F}_D) \cdot \boldsymbol{n}\, dS = 0 \end{aligned} \tag{1}$$

where V is a control volume, $S(V)$ its boundary, and $\boldsymbol{n}$ the outward unit normal. In the general formulation, the equations are written in an inertial frame of reference. The

equations are made non-dimensional with a reference velocity U_∞ and a reference length L_{pp} and the water density ρ.

In equation (1), $\boldsymbol{F}_C$ and $\boldsymbol{F}_D$ represent inviscid (advection and pressure) and diffusive fluxes, respectively:

$$\begin{aligned} \boldsymbol{F}_C &= p\boldsymbol{I} + (\boldsymbol{U} - \boldsymbol{U}_b)\,\boldsymbol{U} \\ \boldsymbol{F}_D &= \left(\frac{1}{Re} + \nu_t\right)\left(\boldsymbol{\nabla U} + \boldsymbol{\nabla U}^T\right) \end{aligned} \tag{2}$$

In the previous equation, $p = P + z/Fr^2$ is the hydrodynamic pressure (i.e. the difference between the total P and the hydrostatic pressure $-z/Fr^2$, $Fr = U_\infty/\sqrt{gL}$ being the Froude number and g the acceleration of gravity parallel to the vertical axis z, positive upward). $\boldsymbol{U}_b$ is the local velocity of the boundary of the control volume, $Re = U_\infty L/\nu$ the Reynolds number, ν the kinematic viscosity, and ν_t the non-dimensional turbulent viscosity; in the present work, the turbulent viscosity has been calculated by means of the one-equation model by Spalart & Allmaras (1994).

The problem is closed by enforcing appropriate conditions at physical and computational boundaries. On solid walls, the relative velocity is set to zero (whereas no condition on the pressure is required); at the (fictitious) inflow boundary, velocity is set to the undisturbed flow value, and pressure is extrapolated from inside; on the contrary, pressure is set to zero at the outflow, whereas velocity is extrapolated from inner points.

At the free surface, whose location is one of the unknowns of the problem, continuity of stresses across the surface is required; if the presence of the air is neglected, the dynamic boundary condition reads:

$$\begin{aligned} p &= \tau_{ij} n_i n_j + \frac{z}{Fr^2} + \frac{\kappa}{We^2} \\ \tau_i j n_i t_j^1 &= 0 \\ \tau_i j n_i t_j^2 &= 0 \end{aligned} \tag{3}$$

where τ_{ij} is the stress tensor, κ is the average curvature, $We = \sqrt{\rho U_\infty^2 L/\sigma}$ is the Weber number (σ being the surface tension coefficient), whereas $\boldsymbol{n}$, $\boldsymbol{t}^1$ and $\boldsymbol{t}^2$ are the surface normal and two tangential unit vectors, respectively.

The actual position of the free surface $F(x, y, z, t) = 0$ is computed from the kinematic condition:

$$\frac{DF(x, y, z, t)}{Dt} = 0 \tag{4}$$

Initial conditions have to be specified for the velocity field and for the free surface configuration:

$$\begin{aligned} u_i\,(x, y, z, 0) &= u_i^0(x, y, z) \quad i = 1, 2, 3 \\ F(x, y, z, 0) &= F^0(x, y, z) \end{aligned} \tag{5}$$

The numerical solution of the governing equations 1 is computed by means of a simulation code developed at CNR-INSEAN; the code yields the numerical solution of the Unsteady Reynolds averaged Navier Stokes equations with proper boundary and initial conditions.

The algorithm is formulated as a finite volume scheme, with variable co-located at cell centers. Turbulent stresses are taken into account by the Boussinesq hypothesis, with several turbulence models (both algebraic and differential) implemented. Free surface effects are taken into account by a single phase level-set algorithm. Complex geometries and multiple bodies in relative motion are handled by a dynamical overlapping grid approach. High performance computing is achieved by an efficient shared and distributed memory parallelization (Broglia *et. al.* (2007) and Broglia *et. al.* (2014)). For more details on the numerical code used the interested reader is referred to Di Mascio *et. al.* (2001, 2007, 2009) and Muscari *et. al.* (2006).

4 RESULTS

The simulations performed in the velocity range $[18-34]$ Knots are carried out on four grid levels: the converged solutions on the three finest grids are sketched in figure (5) in terms of sinkage (left plot) and trim (right plot) and in figure (6) in terms of resistance. A satisfactory convergence of the sinkage is observed for the Froude numbers spanning from 0.7 to 1.1 while some problems are evident for the lowest (≈ 0.6) and the highest (≈ 1.2) Froude where the longer and shorter gravity waves occur, respectively: it is supposed that the coarsest grids are unable to solve in a reliable way the wave pattern produced by the vessel with the consequent over-estimation or under-estimation of the sinkage.

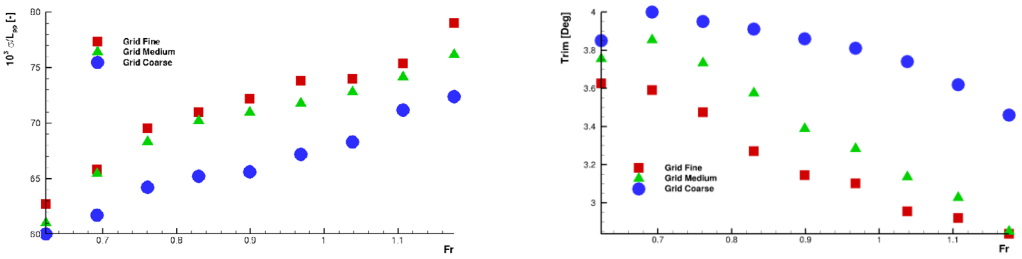

Figure 5: Sinkage (left) and Trim (right) versus Froude number.

The difficulties of the numerical simulations in the correct prevision of the trim angle is a well-known topic and for fast ships may be tricky to overcome, as evident in Akkerman *et. al.* (2012) where a mean error of one degree is appreciable in the simulations performed.

Good convergence properties are also seen for the drag coefficient $C_T = D/(1/2\rho U_\infty^2 L_{pp}^2)$ estimation, reported in figure (6); the worst trends are visible for the lowest and the highest Froude numbers caused by the reasons discussed above regard to the sinkage. It is worth to stress that in the present simulations the towing force, reduced to the center of gravity, possesses a vertical component proportional to the drag force. Therefore, large errors on the drag induce proportional errors on the sinkage, worsening the convergence of the solution for both quantities. For the sake of clearness and to stress the increasing

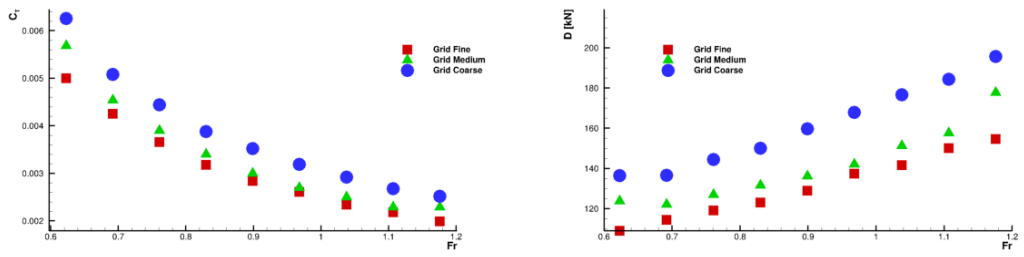

Figure 6: Resistance convergence respect to the Froude number in terms of C_T (left) and dimensional drag (right).

of the total resistance with the Froude number, the dimensional resistance (in KN) is shown in the right plot of figure (6)

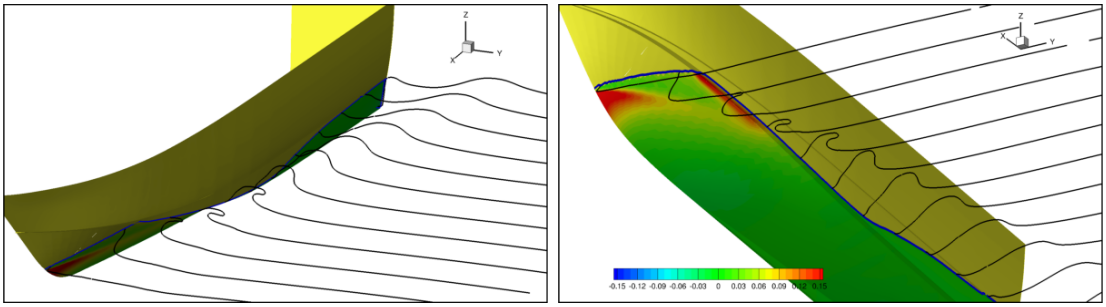

Figure 7: Wave cuts for $Fr \approx 1$ along the hull.

		Extrapolated values			Order of convergence			Uncertainty $U_{SN}(\%S_{RE})$			
Fr	Re	$\sigma/L_{pp}[-]$	$\tau[deg]$	$C_T[-]$	p_σ	p_τ	pC_T	$U_{SN}(\sigma)$	$U_{SN}(\tau)$	$U_{SN}(C_T)$	**Aver.**
0.623	$2.09\,10^8$	$6.327\,10^{-2}$	3.58	$4.773\,10^{-3}$	−0.79	−0.45	−0.23	0.90%	1.21%	4.75%	2.29%
0.692	$2.32\,10^8$	$6.593\,10^{-2}$	3.50	$4.153\,10^{-3}$	3.21	−0.85	0.90	0.20%	2.51%	2.33%	1.68%
0.761	$2.55\,10^8$	$6.991\,10^{-2}$	3.39	$3.580\,10^{-3}$	1.74	−0.24	1.17	0.58%	2.53%	2.23%	1.78%
0.830	$2.78\,10^8$	$7.128\,10^{-2}$	3.17	$3.107\,10^{-3}$	2.56	0.14	1.13	0.39%	3.21%	2.36%	1.99%
0.899	$3.01\,10^8$	$7.262\,10^{-2}$	3.06	$2.787\,10^{-3}$	2.10	0.96	1.70	0.57%	2.64%	1.91%	1.71%
0.969	$3.25\,10^8$	$7.447\,10^{-2}$	3.04	$2.580\,10^{-3}$	1.19	1.54	2.44	0.90%	1.98%	1.16%	1.35%
1.038	$3.48\,10^8$	$7.441\,10^{-2}$	2.90	$2.287\,10^{-3}$	1.88	1.75	1.39	0.55%	2.07%	2.33%	1.65%
1.107	$3.71\,10^8$	$7.582\,10^{-2}$	2.88	$2.143\,10^{-3}$	1.21	2.47	1.83	0.56%	1.24%	1.71%	1.17%
1.176	$3.94\,10^8$	$7.995\,10^{-2}$	2.83	$1.891\,10^{-3}$	0.40	5.67	−0.36	1.19%	0.14%	5.25%	2.19%
							Overall	0.65%	1.95%	2.67%	1.76%

Table 3: Verification study.

Results are summarized in table (3). In the table, extrapolated values (following Roache (1997)) for sinkage, trim and resistance coefficient are reported. Verification assessment is reported as well; the estimation of the order of convergence and the numerical uncertainty (in percentage of the extrapolated value) are reported for all the computed variables. As observed above, good convergence properties are observed for medium speed tests only,

and, primary, for sinkage and resistance computations. Numerical uncertainty is always very low, indicating that a grid converged results are practically achieved (i.e. similar results are obtained on the medium and fine grids). Numerical uncertainty for sinkage prediction is kept below 1% almost for the entire Froude range; larger uncertainty is seen for the trim estimation, with maximum value around 3% and an average (on the speed range) of about 2%. Numerical uncertainty for the resistance prediction shows larger values at the smaller and larger speeds (up to $\sim 5\%$); averaged numerical uncertainty is less than 3%. The overall numerical uncertainty (i.e. averaged over the speed range and the computed variables) is less than 2%.

An analysis of the free surface near the vessel reveals very interesting details. The case $U_\infty = 28Kn$ (i.e. $Fr \approx 1$) is discussed below as an example: same considerations can be drawn for the whole velocity range considered. The figure (7) is obtained through a collection of 12 wave cuts spanning from transom to the bow: the pressure field over the vessel is over-imposed for highlight the areas most stressed on the wetted surface of the hull. As stressed in the introduction, an important feature of the fast ship vessels is the presence of an intense bow jet that is deflected by the hard chines on the boat sides.

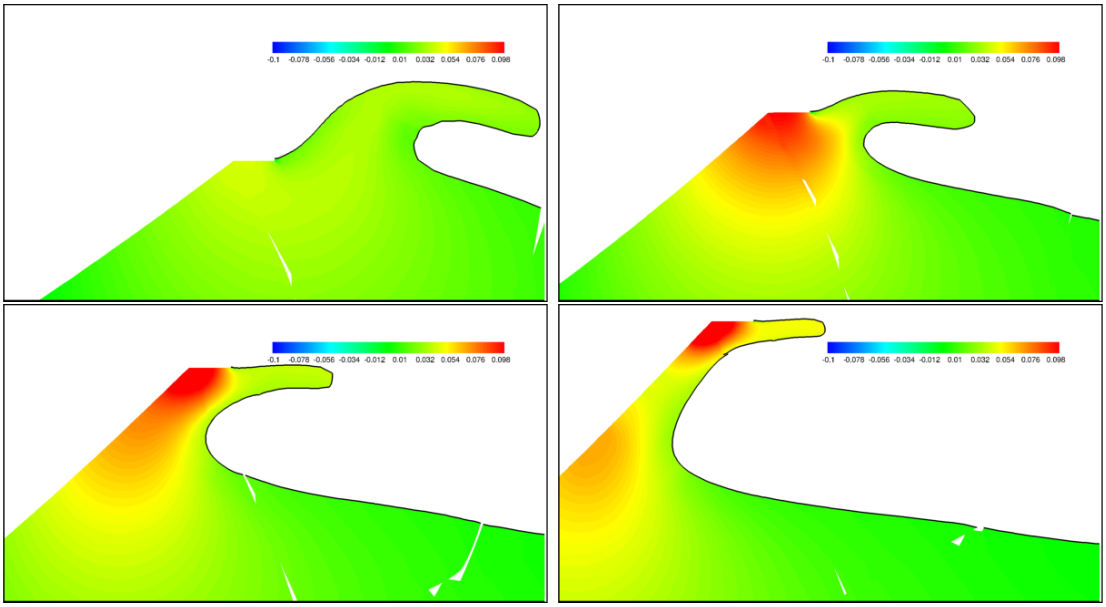

Figure 8: Wave cuts for $Fr \approx 1$ along the hull: magnification of spray for $x/L_{pp} = 0.65$ (top left), 0.7 (top right), 0.75 (bottom left) and 0.8 (bottom right).

From the figure (7) is clearly visible this mechanism that induces an intensive spilling with a consequent bubbles entrapment and the side foam formation. The spilling jet interests about an half of the hull length and some sections (0.65,0.7,0.75,0.8 L_{pp}) are magnified in figure (8): the jet presents a root with an high pressure which justifies the intense area on the side of the hull, visible in the right plot of figure (7) just beneath the

chine. A similar behaviour in a simpler case is described in Durante *et. al.* (2014) where the jet root formed by a planing flat plate is discussed. In the bottom row plots of figure (8), the developing of the jet along the hull when approaching to the bow is depicted. The jet root becomes more intense and finally splits in two structures: a weak jet due to the hull advancing and a second and stronger one due to the impact of the latter with the hard chine (see the right plot in the bottom row of figure (8)).

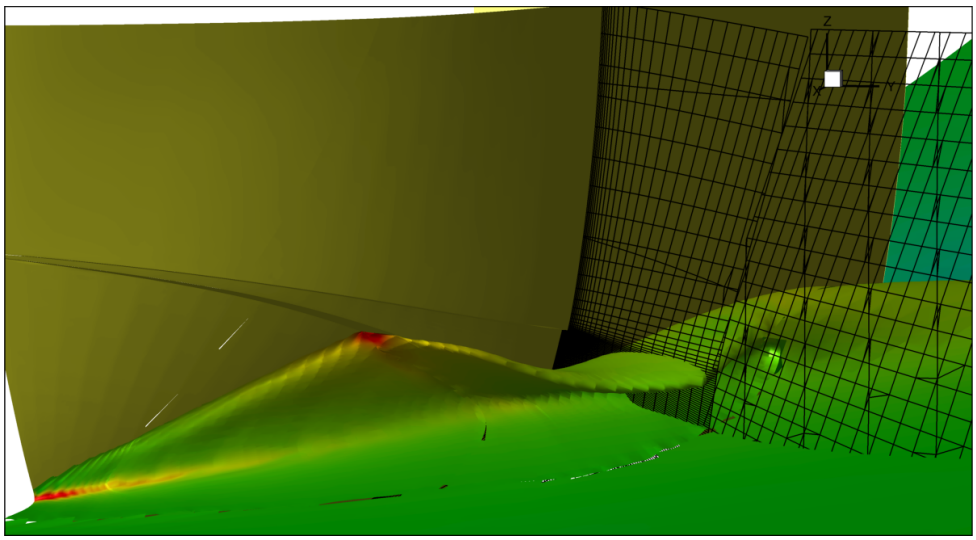

Figure 9: Pressure distribution over the free surface for $Fr \approx 1$ and grid stretching.

A remark on the grid stretching is the purpose of the figure (9), where a slice of the computational mesh near the side wave crest indicates an important change in the cell dimensions from the body-fitted grid to the near wake one. The overlapping grids approach allows an high time machine saving even if the complexity of the breaking of the side jet is lost and will be the matter of the future works. It may be useful to stress how the pressure field over-imposed on the free surface shows again the high pressure areas visible on the hull in figure (7).

5 CONCLUSIONS

In the present paper a study of the trim and sinkage of a semi-displacement vessel is addressed. A chimera overlapping grid approach is exploited in order to describe in a suitable way the flow field generated by the hull with a particular attention placed on the side jet of the hull. Even if the breaking of the jet is not resolved, some important features are well captured such as the hard chine interaction with the primary jet due to the straight motion of the vessel that produces a secondary and more intense jet. The convergence trend of the trim and sinkage is quite satisfactory in the Froude range explored and a particular accuracy is achieved for the mean Froude numbers. Validation

assessment of the straight ahead results, including the comparison with experimental data, and an accurate analysis of the wave pattern in straight motion and in drift, together with a validation of numerical results with the experiments, will be the matter of future activities.

References

Akkerman, I. Dunaway, J. Kvandal, J. Spinks, J. Bazilevs, Y. Toward free-surface modeling of planing vessels: simulation of the Fridsma hull using ALE-VMS. *Computational Mechanics*, **50**: 719–727, 2012.

Begovic, E. Bertorello, C. and Pennino, S. Experimental seakeeping assessment of a warped planing hull model series. *Ocean Engineering*, **83**: 1–15, 2014.

Brizzolara, S. and Serra, F. Accuracy of CFD codes in the prediction of planing surfaces hydrodynamic characteristics. 2^{nd} *International Conference on Marine Research and Transportation*, Ischia, Naples, 2007.

Broglia, R. Di Mascio, A. and Amati, G. A Parallel Unsteady RANS Code for the Numerical Simulations of Free Surface Flows. 2^{nd} *International Conference on Marine Research and Transportation*, Ischia, Naples, 2007.

Broglia, R. Zaghi, S. Muscari, R. and Salvadore, F. Enabling hydrodynamics solver for efficient parallel simulations. *Proc. International Conference on High Performance Computing & Simulation (HPCS)*, July 2014. Bologna, Italy.

Iafrati, A. and Broglia, R. Hydrodynamics of Planing Hulls: a Comparison Between RANS and 2D+t Potential Flow Models. *Proc. of the 2727*$^{\text{th}}$ *Symposium on Naval Hydrodynamics*, Seoul, Korea, 2008.

Broglia, R. and Iafrati, A. Hydrodynamics of Planing Hulls in Asymmetric Conditions. *Proc. of the 28th Symposium on Naval Hydrodynamics*, Pasadena, CA, September 12-17, 2010.

Di Mascio, A. and Broglia, R. and Favini, B. A second order Godunov-type scheme for naval hydrodynamics. Godunov Methods: Theory and Applications, **26**: 253–261, 2001.

Di Mascio, A. and Broglia, R. and Muscari, R. On the application of the single-phase level set method to naval hydrodynamic flows. *Computers and Fluids*, **36**: 868–886, 2007.

Di Mascio, A. and Broglia, R. and Muscari, R. Prediction of hydrodynamic coefficients of ship hulls by high-order Godunov-type methods. *Journal of Marine Science and Technology*, **14**: 19–29, 2009.

Durante, D. Broglia, R. Maki, K. J. Di Mascio, A. A study on the effect of the cushion pressure on a planing surface. *Ocean Engineering*, **91**: 122–132, 2014.

Favini, B. and Broglia, R. and Di Mascio, A. Multigrid acceleration of second-order ENO schemes from low subsonic to high supersonic flows. *International Journal for Numerical Methods in Fluids*, **23**: 589–606, 1996.

Fu, T.C. O'Shea, T.T. Judge, C.Q. Dommermuth, D. Brucker, K.A. and Wyatt, D.C. A Detailed Assessment of Numerical Flow Analysis (NFA) to Predict the Hydrodynamics of a Deep-V Planing Hull. *Proc. of the* 29^{th} *Symposium on Naval Hydrodynamics*, Gothenburg, Sweden, August 26-31, 2012.

Fu, T.C. Brucker, K.A. Mousaviraad, S.M. Ikeda, C.M. Lee, E.J. O'Shea, T.T. Wang, Z. Stern, F. and Judge, C.Q. An Assessment of Computational Fluid Dynamics Predictions of the Hydrodynamics of High-Speed Planing Craft in Calm Water and Waves. *Proc. of the* 30^{th} *Symposium on Naval Hydrodynamics*, Hobart, Tasmania, November 2-7, 2014.

Judge, C. Q. and Ikeda, C. M. An An Experimental Study of Planing Hull Wave Slam Events. *Proc. of the* 30^{th} *Symposium on Naval Hydrodynamics*, Hobart, Tasmania, November 2-7, 2014.

Landrini, M. Colagrossi, A. Greco, M. Tulin, M.P. The fluid mechanics of splashing bow waves on ships: A hybrid BEM-SPH analysis. *Ocean Engineering*, **53**: 111–127, 2012.

Muscari, R. and Broglia, R. and Di Mascio, A. An overlapping grids approach for moving bodies problems. 16^{th} *International Offshore and Offshore and Polar Engineering Conference Proceedings*, isbn: 1880653664, 2006.

Pérez-Arribas, F. Parametric generation of planing hulls. *Ocean Engineering*, **81**: 89–104, 2014.

Spalart, P.R. and Allmaras, S.R. A one-equation turbulence model for aerodynamic flows. La Recherce Aerospatiale, **1**: 5–21, 1994.

Roache, P.J. Quantification of Uncertainty in Computational Fluid Dynamics. Ann. Rev. Fluid Mech., **29**: 123–160, 1997.